

<sup>1</sup> **neonSoilFlux: An R Package for Continuous  
2 Sensor-Based Estimation of Soil CO<sub>2</sub> Fluxes**

<sup>3</sup> John Zobitz<sup>1</sup>      Edward Ayres<sup>2</sup>      Zoey Werbin<sup>3</sup>      Ridwan Abdi<sup>1</sup>  
<sup>4</sup>                         Natalie Ashburner-Wright<sup>4,5</sup>      Lillian Brown<sup>4,5</sup>  
<sup>5</sup>                         Ryan Frink-Sobierajski<sup>4,5</sup>      Lajntxiag Lee<sup>1</sup>      Dijonë Mehmeti<sup>1</sup>  
<sup>6</sup>                         Christina Tran<sup>4,5</sup>      Ly Xiong<sup>1</sup>      Naupaka Zimmerman<sup>4,5</sup>

<sup>7</sup> <sup>1</sup> Augsburg University, 2211 Riverside Avenue, Minneapolis, MN 55454

<sup>8</sup> <sup>2</sup> National Ecological Observatory Network, Battelle, 1685 38th Street, Suite 100, Boulder, CO  
<sup>9</sup> 80301

<sup>10</sup> <sup>3</sup> Boston University, 5 Cummington Street, Boston, MA 02215

<sup>11</sup> <sup>4</sup> University of [Kansas, 1450 Jayhawk Boulevard, Lawrence, KS 66045](#)

<sup>12</sup> <sup>5</sup> [University of](#) San Francisco, 2130 Fulton Street, San Francisco, CA 94117 <sup>5</sup> [University of](#)  
<sup>13</sup> [Kansas, 1450 Jayhawk Boulevard, Lawrence, KS 66045](#)

<sup>14</sup> **Acknowledgments**

<sup>15</sup> [JZ—John Zobitz](#) acknowledges Kathleen O'Rourke for code development. [NZ—Naupaka](#)

<sup>16</sup> [Zimmerman](#) thanks technical staff at USF for support with field gear assembly and shipping.

17 We thank the NEON field staff and assignable assets teams for facilitating each of the six  
18 NEON site visits. We are grateful to LI-COR technical staff for helpful discussions about  
19 optimal soil chamber sampling methods. This work was supported by NSF DEB grant  
20 #2017829 awarded to JZJohn Zobitz, and NSF DEB grant #2017860 awarded to NZNaupaka  
21 Zimmerman. This material is based in part upon work supported by the National Ecological  
22 Observatory Network (NEON), a program sponsored by the U.S. National Science Foundation  
23 (NSF) and operated under cooperative agreement by Battelle. We also thank the reviewers  
24 and subject editor for their constructive feedback.

## 25 **Conflict of Interest Statements**

26 None of the authors have a financial, personal, or professional conflict of interest related to this  
27 work.

## 28 **Author Contributions**

29 Conceptualization: JZ, NZJohn Zobitz, Naupaka Zimmerman; Methodology: EA, JZ,  
30 NZEdward Ayres, John Zobitz, Naupaka Zimmerman; Software: JZ, NZ, ZW, E A, DM,  
31 RA, LX, LLJohn Zobitz, Naupaka Zimmerman, Zoey Werbin, Edward Ayres, Dijonë  
32 Mehmeti, Ridwan Abdi, Ly Xiong, Lajntxiag Lee; Validation: JZ, NZJohn Zobitz, Naupaka  
33 Zimmerman; Formal Analysis: JZ, NZ, DM, RA, LX, LLJohn Zobitz, Naupaka Zimmerman,  
34 Dijonë Mehmeti, Ridwan Abdi, Ly Xiong, Lajntxiag Lee; Investigation: JZ, NZ, RF-S,  
35 CT, NA-W, LBJohn Zobitz, Naupaka Zimmerman, Ryan Frink-Sobierajski, Christina  
36 Tran, Natalie Ashburner-Wright, Lillian Brown; Resources: JZ, NZJohn Zobitz, Naupaka  
37 Zimmerman; Data curation: JZ, NZ, DM, LXJohn Zobitz, Naupaka Zimmerman, Dijonë

38 Mehmeti, Ly Xiong; Writing – original draft: JZ, NZ John Zobitz, Naupaka Zimmerman; Writ-  
39 ing – review and editing: JZ, NZ, ZW, EA, CT, DM, LX, John Zobitz, Naupaka Zimmerman,  
40 Zoey Werbin, Edward Ayres, Christina Tran, Dijoné Mehmeti, Ly Xiong; Visualization: JZ,  
41 NZ, DM, RA, LX, John Zobitz, Naupaka Zimmerman, Dijoné Mehmeti, Ridwan Abdi, Ly  
42 Xiong; Supervision: JZ, NZ, John Zobitz, Naupaka Zimmerman; Project Administration: JZ;  
43 NZ, John Zobitz, Naupaka Zimmerman; Funding Acquisition: JZ, NZ, John Zobitz, Naupaka  
44 Zimmerman.

## 45 Data Availability

46 ~~Anonymous field-collected Data available via https://doi.org/10.5281/zenodo.17516319 (Zobitz~~  
47 ~~& Zimmerman, 2025). Field-collected data, neonSoilFlux calculated outputs, and manuscript-~~  
48 ~~generating code for peer review are provided as supplemental files. An anonymous link for~~  
49 ~~peer review is here: . This will be made publicly available upon publication. are provided~~  
50 ~~within this repository.~~

51 **1 Abstract**

- 52 1. Accurate quantification of soil carbon fluxes is essential to reduce uncertainty in estimates  
53 of the terrestrial carbon sink. However, these fluxes vary over time and across ecosystem  
54 types and so it can be difficult to estimate them accurately across large scales. The flux  
55 gradient method estimates soil carbon fluxes using co-located measurements of soil CO<sub>2</sub>  
56 concentration, soil temperature, soil moisture, and other soil properties. The National  
57 Ecological Observatory Network (NEON) provides such data across 20 ecoclimatic domains  
58 spanning the continental U.S., Puerto Rico, Alaska, and Hawai‘i.
- 59 2. We present an R software package (`neonSoilFlux`) that acquires soil environmental data  
60 to compute half-hourly soil carbon fluxes for each soil replicate plot at a given terrestrial  
61 NEON site. To assess the computed fluxes, we visited six focal NEON sites and measured  
62 soil carbon fluxes using a closed-dynamic chamber approach.
- 63 3. Outputs from the `neonSoilFlux` showed agreement with measured fluxes ( $R^2$  between  
64 measured and `neonSoilFlux` outputs ranging from ~~0.04 to 0.81~~ 0.12 to 0.77 depending on  
65 calculation method used); measured outputs generally fell within the range of calculated  
66 uncertainties from the gradient method. Calculated fluxes from `neonSoilFlux` aggregated  
67 to the daily scale exhibited expected site-specific seasonal patterns.
- 68 4. While the flux gradient method is broadly effective, its accuracy is highly sensitive  
69 to site-specific inputs, including the extent to which gap-filling techniques are used to  
70 interpolate missing sensor data and to estimates of soil diffusivity and moisture content.  
71 Future refinement and validation of `neonSoilFlux` outputs can contribute to existing  
72 databases of soil carbon flux measurements, providing near real-time estimates of a critical  
73 component of the terrestrial carbon cycle.

<sup>74</sup> **1.1 Keywords**

<sup>75</sup> Soil carbon, carbon dioxide, flux gradient, carbon cycle, field validation, soil respiration,  
<sup>76</sup> ecosystem variability, diffusion

<sup>77</sup> **2 Data for peer review**

<sup>78</sup> ~~Anonymous field-collected data, neonSoilFlux calculated outputs, and manuscript-generating~~  
<sup>79</sup> ~~code for peer review are provided as supplemental files. An anonymous link for peer review is~~  
<sup>80</sup> ~~here: . This will be made publicly available upon publication.~~

<sup>81</sup> **2 Introduction**

<sup>82</sup> Soils contain the planet's largest reservoir of terrestrial carbon (Jobbágy & Jackson, 2000). A  
<sup>83</sup> critical component of this reservoir is soil organic matter, the accumulation of which is influenced  
<sup>84</sup> by biotic factors such as above-ground plant inputs (Jackson et al., 2017). These inputs in  
<sup>85</sup> turn are influenced by environmental factors such as growing season length, temperature, and  
<sup>86</sup> moisture (Desai et al., 2022), which also affect the breakdown of soil organic matter and its  
<sup>87</sup> return to the atmosphere. Across heterogeneous terrestrial landscapes, the interplay between  
<sup>88</sup> these biotic and abiotic factors influence the size of the soil contribution to the terrestrial  
<sup>89</sup> carbon sink (Friedlingstein et al., 2025). However, the heterogeneity of these processes across  
<sup>90</sup> diverse ecosystems in the context of rapid environmental change leads to large uncertainty  
<sup>91</sup> about the magnitude of this sink in the future, and thus there remains a pressing need to  
<sup>92</sup> quantify changes in soil carbon pools and fluxes across scales.

93 Ecological observation networks such as the United States' National Ecological Observatory  
94 Network (NEON) and others (e.g. the globally-distributed FLUXNET or the European Inte-  
95 grated Carbon Observation System) present a significant advancement in the nearly continuous  
96 observation of biogeochemical processes at the continental scale. Notably, at 47 terrestrial  
97 sites across the continental United States that span 20 ecoclimatic domains, NEON provides  
98 half-hourly measurements of soil CO<sub>2</sub> concentration, temperature, and moisture at different  
99 vertical depths. Each of these NEON sites also encompasses measurements of the cumulative  
100 sum of all ecosystem carbon fluxes in an airshed using the eddy covariance technique (Baldocchi,  
101 2014). Soil observations provided by NEON are on the same timescale and standardized with  
102 eddy covariance measurements from FLUXNET. These types of nearly continuous observational  
103 data (NEON and FLUXNET) can be used to reconcile differences between model-derived  
104 or data-estimated components of ecosystem carbon flux (Jian et al., 2022; Luo et al., 2011;  
105 Phillips et al., 2017; J. Shao et al., 2015; P. Shao et al., 2013; Sihi et al., 2016).

106 Estimated or observed soil carbon fluxes are a key metric for understanding change in soil  
107 carbon pools over time (Bond-Lamberty et al., 2024). A soil carbon flux to the atmosphere ( $F_S$ ,  
108 units  $\mu\text{mol m}^{-2} \text{s}^{-1}$ ), represents the aggregate process of transfer of soil CO<sub>2</sub> to the atmosphere  
109 from physical and biological processes (e.g. diffusion and respiration). Soil carbon fluxes can  
110 be assumed to encompass soil carbon respiration from autotrophic or heterotrophic sources  
111 (Davidson et al., 2006) and modeled with a exponential  $Q_{10}$  paradigm (Bond-Lamberty et al.,  
112 2004; Chen & Tian, 2005; Hamdi et al., 2013).

113 One common method by which  $F_S$  is measured in the field is through the use of soil chambers  
114 in a closed, well-mixed system (Norman et al., 1997) with headspace trace gas concentrations  
115 measured with an infrared gas analyzer (IRGA).  $F_S$  can also be estimated from soil CO<sub>2</sub>  
116 measurements at different depths in the soil using the flux-gradient method (Maier & Schack-  
117 Kirchner, 2014). Closed-chamber IRGA measurements, while being the most common method,

118 require either frequent in-person site visits or expensive and fragile automated systems. The  
119 potential of the gradient method is that fluxes can be estimated from continuous data recorded  
120 by robust solid-state sensors. The flux-gradient method is an approach that uses conservation of  
121 mass to calculate flux at a vertical soil depth  $z$  at steady state by applying Fick's law of diffusion.  
122 A simplifying assumption for the flux-gradient method is that there is no mass transfer in the  
123 other spatial dimensions  $x$  and  $y$  (Maier & Schack-Kirchner, 2014). The diffusivity profile, a  
124 key component of this calculation, varies across the soil depth as a function of soil temperature,  
125 soil volumetric water content, atmospheric air pressure, and soil bulk density (Millington &  
126 Shearer, 1971; Moldrup et al., 1999; Sallam et al., 1984).

127 Databases such as the Soil Respiration Database (SRDB) or the Continuous Soil Respiration  
128 Database (COSORE) add to the growing network of resources for making collected observations  
129 of soil fluxes available to other researchers (Bond-Lamberty, 2018; Bond-Lamberty et al., 2020;  
130 Bond-Lamberty & Thomson, 2010; Jian et al., 2021; Jiang et al., 2024). However, these  
131 databases currently encompass primarily direct soil measurements of fluxes (i.e. those using  
132 methods like the closed-chamber method described above). Currently, NEON provides all  
133 measurements to calculate  $F_S$  from Fick's law, but soil flux as a derived data product was  
134 descoped from the initial network launch due to budget constraints (Berenbaum et al., 2015).  
135 Deriving estimates of  $F_S$  using continuous sensor data across NEON sites [using NEON data](#)  
136 thus remains a high priority.

137 This study describes an R software package, `neonSoilFlux`, that computes a standardized  
138 estimate of  $F_S$  at all terrestrial NEON sites using the flux-gradient method. Using direct  
139 chamber-based field observations of soil carbon dioxide flux from a subset of terrestrial NEON  
140 sites spanning six states, we provide a direct validation of  $F_S$  from `neonSoilFlux`. [While](#)  
141 [open source R software tools currently exist for processing chamber-based flux measurements](#)  
142 [\(Jurasinski et al., 2022; Pedersen, 2024; Rheault et al., 2024; Wilson et al., 2024; Zhao, 2019\)](#).

<sup>143</sup> to our knowledge this is the first package that incorporates NEON data directly.

<sup>144</sup> Key objectives of this study are to:

- <sup>145</sup> 1. Apply the flux-gradient method to estimate soil CO<sub>2</sub> flux from continuous sensor mea-
- <sup>146</sup> surements across six NEON sites.
- <sup>147</sup> 2. Benchmark estimated soil carbon fluxes against field measurements (e.g. direct chamber
- <sup>148</sup> measurements of soil flux).
- <sup>149</sup> 3. Identify sources of error in the flux-gradient approach across diverse sites in order to
- <sup>150</sup> guide future work.

### <sup>151</sup> 3 Materials and Methods

#### <sup>152</sup> 3.1 Field methods

##### <sup>153</sup> 3.1.1 Focal NEON Sites

<sup>154</sup> In order to acquire field data to validate model predictions of flux, we selected six terrestrial  
<sup>155</sup> NEON sites for analysis. We conducted roughly week-long field measurement campaigns at  
<sup>156</sup> these sites, which span a range of environmental gradients and terrestrial domains (Table 1).  
<sup>157</sup> SJER, SRER, and WREF were visited during May and June of 2022, and WOOD, KONZ, and  
<sup>158</sup> UNDE during May and June of 2024. Permits or waivers were sought and approved prior to  
<sup>159</sup> field work at all six sites. In 2022, research activities were conducted whole or in part on the  
<sup>160</sup> Wind River Experimental Forest within the Gifford Pinchot National Forest. No permit was  
<sup>161</sup> required for this work. Approval for research at San Joaquin Experimental Range was granted  
<sup>162</sup> by Dr. Angela White in May 2022 and for research at Santa Rita Experimental Range by  
<sup>163</sup> Dr. Mitch McClaran in May 2022. In 2024, permits were received for work at WOOD (Chase

164 Lake WMD; permit number 62515-24-020), KONZ (Konza Prairie Biological Station; permit  
165 number 766), and UNDE (University of Notre Dame Environmental Research Center; permit  
166 number UNDERC-2024-5).

**167 3.1.2 Soil collar placement**

168 Either one (2022 sampling campaign) or two (2024 sampling campaign) PVC soil collars (20.1  
169 cm inside diameter) were installed in close proximity to the permanent NEON soil sensors at  
170 each site (Figure 1). As instruments in the NEON soil sensor arrays can occasionally break  
171 down or stop working, the specific soil plot where we made measurements was chosen at each  
172 site in consultation with NEON staff to maximize likelihood of quality soil sensor measurements  
173 during the duration of the IRGA measurements. The plot selected at each site (out of the 5 in  
174 each replicate array at each site) are presented in the last column of Table 1. After installation,  
175 collar(s) were left to equilibrate for approximately 24 hours prior to any measurements being  
176 taken.

**177 3.1.3 Infrared gas analyzer measurements of soil CO<sub>2</sub> flux**

178 In 2022, we then made measurements of flux on an hourly interval for 8 hours each day.  
179 Measurements were taken from roughly 8 am to 4 pm, with the time interval selected to  
180 capture the majority of the diurnal gradient of soil temperature each day. These measurements  
181 were made using a LI-6800 infrared gas analyzer instrument (LI-COR Environmental, Lincoln,  
182 NE) fitted with a soil chamber attachment (attachment 6800-09). In 2024, we again used the  
183 same LI-6800 instrument, but made half-hourly measurements over an approximately 8 hour  
184 period. In addition, in 2024 we also installed a second collar and used a second instrument, an  
185 LI-870 CO<sub>2</sub> IRGA, connected to an automated robotic chamber (LI-COR chamber 8200-104)

186 controlled by an LI-8250 multiplexer to make automated measurements. The multiplexer was  
187 configured to take half-hourly measurements 24 hours a day for the duration of our sampling  
188 bout at each site. Each instrument was paired with a soil temperature and moisture probe  
189 (Stevens HydraProbe, Stevens Water, Portland, OR) that was used to make soil temperature  
190 and moisture measurements concurrent with the CO<sub>2</sub> flux measurements. Chamber volumes  
191 were set by measuring collar offsets at each site. System checks were conducted daily for the  
192 LI-6800 and weekly for the LI-8250. Instruments were factory calibrated before each field  
193 season.

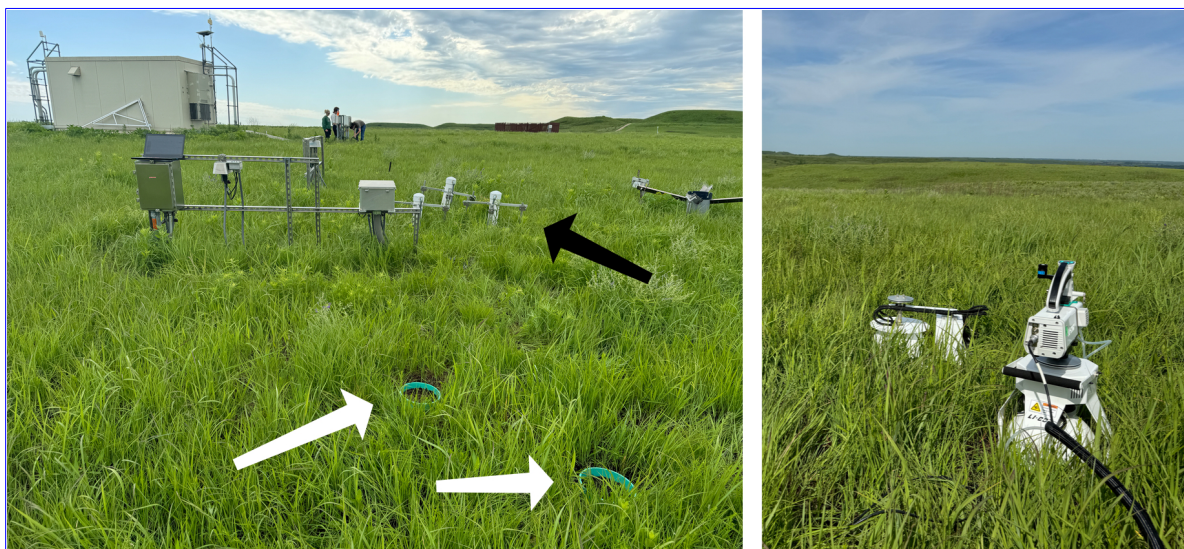


Figure 1: Spatial layout of field sampling using a closed-dynamic chamber setup at a representative NEON site (KONZ). Left image shows collars (white arrows) and permanent soil sensor installation (black arrow) and right image shows the LI-6800 (foreground) and LI-8200-104 (background) instruments placed on the collars.

g of NEON sites studied for field work and analysis. Site refers to NEON site ID: Santa Rita Experimental Range (SRER), San Joaquin Experimental Range (SJER), Wind River Experimental Forest (WREF), Chase Lake National Wildlife Refuge (WOOD), Konza Prairie Biological Station (KONZ), and the University of Notre Dame Environmental Research Center (UNDE). Location is reported in decimal degrees of latitude and longitude. Other abbreviations include Mean Annual Temperature (MAT);  $\overline{T_S}$ : average soil temperature during field measurements;  $\overline{SWC}$ : average soil water content during field measurements. Dates refer to field measurement dates for each site. Plot refers to the particular location in the soil sensor array (labeled as HOR by NEON) where field measurements were made.

Site	Location	Ecosystem	MAT	$\overline{T_S}$	MAP	$\overline{SWC}$	Dates	Plot
SRER	31.91068, -110.83549	Shrubland	19.3 °C	47.6 °C	346 mm	4.0%	May 29– June 1 2022	004
SJER	37.10878, -119.73228	Oak woodland	16.4 °C	41.7 °C	540 mm	1.2%	June 1–4 2022	005
WREF	45.82049, -121.95191	Evergreen forest	9.2 °C	15.3 °C	2225 mm	27.2%	June 7–9 2022	001
WOOD	47.1282, -99.241334	Restored prairie	4.9 °C	14.9 °C	495 mm	14.9%	June 3–9 2024	001
KONZ	39.100774, -96.563075	Tallgrass prairie	12.4 °C	23.4 °C	870 mm	23.4%	May 29– June 1 2024	001
UNDE	46.23391, -89.537254	Deciduous forest	4.3 °C	13.0 °C	802 mm	13.0%	May 22–25 2024	004

### 3.1.4 Post-collection processing of field data

We used LI-COR SoilFluxPro software (v 5.3.1) to assess the data after collection and to inform sampling parameters. We checked appropriateness of dead band and measurement durations using built-in evaluation tools. Based on this, the deadband period was set for 30-40 seconds, depending on the site, and the measurement duration was 180 seconds with a 30 second pre-purge and a 30 second post-purge at most sites, and a 90 second pre- and post-purge at sites with higher humidity due to recent precipitation events. We also assessed the  $R^2$  of linear and exponential model fits to measured CO<sub>2</sub> to verify measurement quality.

202 **3.2 neonSoilFlux R package**

203 We developed an R package called `neonSoilFlux` (Zobitz et al., 2024) to compute half-hourly  
204 soil carbon fluxes and uncertainties from NEON data. The objective of the `neonSoilFlux`  
205 package is a unified workflow (Figure 2) for soil data acquisition and analysis that supplements  
206 the existing `neonUtilities` data acquisition R package (Lunch et al., 2025).

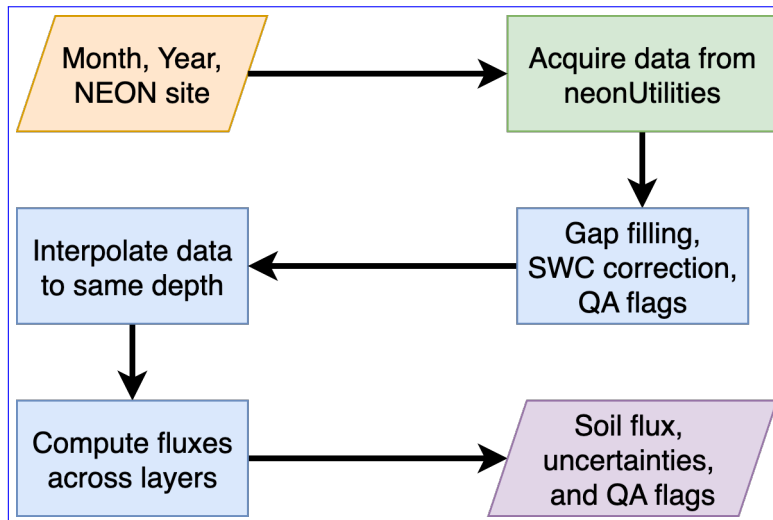


Figure 2: Diagram of `neonSoilFlux` R package. For a given month, year, and NEON site (orange parallelogram), the package acquires all relevant data to compute  $F_S$  using the `neonUtilities` R package (green rectangle). Data are gap-filled according to reported QA flags and adjusted for changes in soil water content (SWC) calibration coefficients, then interpolated to the same measurement depth before computing the soil flux, uncertainties, and final QA flags (blue rectangles). The package reports the associated soil flux, uncertainties, and quality assurance (QA) flags for the user (purple parallelogram).

207 At a given NEON site there are five replicate soil plots, each with measurements of soil  
208 CO<sub>2</sub> concentration, soil temperature, and soil moisture at different depths (Figure 3).  
209 The `neonSoilFlux` package acquires measured soil CO<sub>2</sub> concentration ([National Ecological  
210 Observatory Network \(NEON\) NEON](#), 2024b), soil temperature ([National Ecological  
211 Observatory Network \(NEON\) NEON](#), 2024d), soil water content ([National Ecological](#)

212 Observatory Network (NEON)NEON, 2024e), barometric pressure from the nearby tower  
 213 (National Ecological Observatory Network (NEON)NEON, 2024a), and soil properties  
 214 (e.g. bulk density) (National Ecological Observatory Network (NEON)NEON, 2024c) from a  
 215 range of different NEON data products. The static soil properties were collected by NEON  
 216 staff from a nearby soil pit during initial site characterization and are assumed to be constant  
 217 at each site. A soil flux calculation is computed at each replicate soil plot.

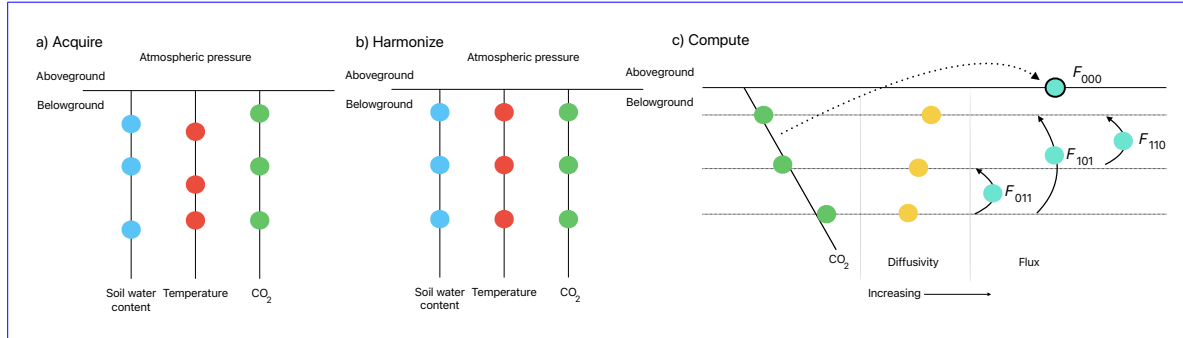


Figure 3: Model diagram of the data workflow for the `neonSoilFlux` R package. a) Acquire: Data are obtained for a given NEON location and horizontal sensor location, which includes soil water content, soil temperature,  $\text{CO}_2$  concentration, and atmospheric pressure. All data are screened for quality assurance; if gap-filling of missing data occurs, it is flagged for the user. b) Harmonize: Any belowground data are then harmonized to the same depth as  $\text{CO}_2$  concentrations using linear regression. c) Compute: The flux across a given depth is computed via Fick's law, denoted with  $F_{ijk}$ , where  $i$ ,  $j$ , or  $k$  are either 0 or 1 denoting the layers the flux is computed across ( $i = \text{closest to surface}$ ,  $k = \text{deepest}$ ).  $F_{000}$  represents a flux estimate where the gradient  $dC/dz$  is the slope of a linear regression of  $\text{CO}_2$  with depth.

218 The workflow to compute a value of  $F_S$  with `neonSoilFlux` consists of three primary steps,  
 219 illustrated in Figure 3. First, NEON data are acquired for a given site and month via the  
 220 `neonUtilities` R package (yellow parallelogram and green rectangle in Figure 2 and Panel  
 221 a in Figure 3). Acquired environmental data can be exported to a comma separated value  
 222 file for additional analysis. Quality assurance (QA) flags are reported as an indicator variable.  
 223 Since the calibration coefficients on the soil water content sensors have changed over time  
 224 (National Ecological Observatory Network (NEON)NEON, 2024e), raw sensor measurements

were back-calculated and soil-specific calibrations were applied following Ayres et al. (2024) to generate a consistent time series at each measurement location.

The second step is harmonizing the data to compute soil fluxes across soil layers. This step consists of three different actions (blue rectangles in Figure 2 and Panel b in Figure 3). If a given observation by NEON is reported as not passing a quality assurance check, we applied a gap filling method to replace that measurement with its monthly mean at that same depth (Section 3.2.1). Belowground measurements of soil water and soil temperature are then interpolated to the same depth as soil CO<sub>2</sub> measurements. The diffusivity (Section 3.2.2) and soil flux across different soil layers (Section 3.2.3) are then computed.

The third and final step is computing a surface soil flux through extrapolation to the surface (purple parallelogram in Figure 2 and Panel c in Figure 3). Uncertainty on a soil flux measurement is computed through quadrature. An aggregate quality assurance (QA) flag for each environmental measurement is also reported, representing if any gap-filled measurements were used in the computation of a soil flux. Within the soil flux-gradient method, several different approaches can be used to derive a surface flux (Maier & Schack-Kirchner, 2014); the `neonSoilFlux` package reports four different possible values for soil surface flux (Section 3.2.3) for each of two different methods of diffusivity estimation, for a total of eight estimates of flux.

### 3.2.1 Gap-filling routine

NEON reports QA flags as binary values for each measurement and half-hourly interval. For a given half-hour, if any input variable (soil CO<sub>2</sub> concentration, soil temperature, or soil moisture) at depth  $z$  is flagged, computation of  $F_S$  is not possible. To address this, flagged measurements

and their uncertainties were replaced with a bootstrapped monthly mean ( $\bar{m}$ ) and monthly standard deviation ( $\bar{s}$ ) (Efron & Tibshirani, 1994).

For each month, depth  $z$ , and variable, we computed bootstrapped estimates of  $\bar{m}$  and  $\bar{s}$  from the vectors of unflagged measurements ( $\mathbf{m}$ ), reported standard errors ( $\sigma$ ), and the 95% confidence interval ( $\epsilon$ , or expanded uncertainty; Farrance & Frenkel (2012)). We also defined a bias vector  $\mathbf{b} = \sqrt{\epsilon^2 - \sigma^2}$ , which quantifies the spread of uncertainty in a given period and is incorporated into  $\bar{m}$ .

From these, 5000 bootstrap samples were generated for  $\mathbf{m}$ ,  $\sigma$ , and  $\mathbf{b}$ . For each sample  $(m_k, b_k, \sigma_k)$ , we generated a vector  $\mathbf{n}$  (length  $N = 5000$ ) by drawing from a normal distribution with mean  $m_k + b_k$  and standard deviation  $\sigma_k$ . The sample mean and standard deviation were then computed from  $\mathbf{n}$ . The resulting distributions of sample means and sample standard deviations provided the bootstrapped monthly mean ( $\bar{m}$ ) and standard error ( $\bar{s}$ ) respectively.

This gap-filling procedure provides a consistent treatment across all data streams. However, alternative approaches may be better suited for longer gaps (e.g., correlations with other NEON measurement levels or soil plots) or for variable-specific conditions. We discuss the effect of gap-filling on our results in Section 5.1.

### 3.2.2 Soil diffusivity

Soil diffusivity  $D_a$  at a given measurement depth is the product of the diffusivity in free air  $D_{a,0}$  ( $\text{m}^2 \text{ s}^{-1}$ ) and the tortuosity  $\xi$  (no units) (Millington & Shearer, 1971).

We compute  $D_{a,0}$  with Equation 1:

$$D_{a,0} = 0.0000147 \cdot \left( \frac{T_i + 273.15}{293.15} \right)^{1.75} \cdot \left( \frac{P}{101.3} \right) \quad (1)$$

267 where  $T_i$  is soil temperature ( $^{\circ}\text{C}$ ) at depth  $i$  (National Ecological Observatory Network  
268 (NEON)NEON, 2024d) and  $P$  surface barometric pressure (kPa) (National Ecological  
269 Observatory Network (NEON)NEON, 2024a).

270 Previous studies by Sallam et al. (1984) and Tang et al. (2003) demonstrated the sensitivity  
271 of modeled  $F_S$  depending on the tortuosity model ( $\xi$ ) used to compute diffusivity. At low  
272 soil water content, the choice of tortuosity model can lead to order-of-magnitude differences  
273 in  $D_a$ , which in turn affect modeled  $F_S$ . The neonSoilFlux package currently includes two  
274 approaches to calculate  $\xi$ , representing the range of tortuosity behavior reported in Sallam et  
275 al. (1984).

276 The first approach is the Millington-Quirk model (Millington & Shearer, 1971), in which  
277 tortuosity depends on both porosity and soil water content:

$$\xi = \frac{(\phi - SWC_i)^{10/3}}{\phi^2} \quad (2)$$

278 In Equation 2,  $SWC$  is the soil water content at depth  $i$  (National Ecological Observatory  
279 Network (NEON)NEON, 2024e) and  $\phi$  is the porosity, which in turn is a function of soil  
280 physical properties (National Ecological Observatory Network (NEON)NEON, 2024c):

$$\phi = \left(1 - \frac{\rho_s}{\rho_m}\right) (1 - f_V) \quad (3)$$

281 In Equation 3,  $\rho_m$  is the particle density of mineral soil ( $2.65 \text{ g cm}^{-3}$ ),  $\rho_s$  the soil bulk density ( $\text{g}$   
282  $\text{cm}^{-3}$ ) excluding coarse fragments greater than 2 mm (National Ecological Observatory Network  
283 (NEON)NEON, 2024c), and  $f_V$  is a site-specific value that accounts for the proportion of  
284 soil fragments between 2-20 mm. Soil fragments greater than 20 mm were not estimated due

285 to limitations in the amount of soil that can be analyzed ([National Ecological Observatory](#)  
286 [Network \(NEON\)](#)[NEON](#), 2024c). We assume that rock fragments contain no internal pores.

287 The Millington-Quirk model assumes  $\xi$  is modulated by the amount of fluid saturation in soil  
288 pores (Millington & Shearer, 1971). In contrast, the Marshall model (Marshall, 1959) expresses  
289 tortuosity as only a function of porosity ( $\xi = \phi^{1.5}$ ), with  $\phi$  defined from Equation 3. The  
290 Marshall model is independent of soil water content and assumes tortuosity is only governed  
291 by soil structure. The `neonSoilFlux` package allows users to choose the tortuosity model most  
292 appropriate for site-specific conditions and research goals.

293 **3.2.3 Soil flux computation**

294 We applied Fick's law (Equation 4) to compute the soil flux  $F_{ij}$  ( $\mu\text{mol m}^{-2} \text{s}^{-1}$ ) across two  
295 soil depths  $i$  and  $j$ :

$$F_{ij} = -D_a \frac{dC}{dz} \quad (4)$$

296 where  $D_a$  is the diffusivity ( $\text{m}^2 \text{s}^{-1}$ ) and  $\frac{dC}{dz}$  is the gradient of CO<sub>2</sub> molar concentration ( $\mu\text{mol}$   
297  $\text{m}^{-3}$ , so the gradient has units of  $\mu\text{mol m}^{-3} \text{m}^{-1}$ ). The soil surface flux is theoretically defined  
298 by applying Equation 4 to measurements collected at the soil surface and directly below the  
299 surface. Measurements of soil temperature, soil water content, and soil CO<sub>2</sub> molar concentration  
300 across the soil profile allow for application of Equation 4 across different soil depths. Each  
301 site had three measurement layers, so we denote the flux as a three-digit subscript  $F_{ijk}$  with  
302 indicator variables  $i$ ,  $j$ , and  $k$  indicate if a given layer was used (written in order of increasing  
303 depth), according to the following:

- $F_{000}$  is a surface flux estimate using the intercept of the linear regression of  $D_a$  with depth and the slope from the linear regression of CO<sub>2</sub> with depth (which represents  $\frac{dC}{dz}$  in Fick's Law). Tang et al. (2003) used this approach to compute fluxes in an oak-grass savannah.
- $F_{110}$  is a flux estimate across the two shallowest measurement layers.
- $F_{011}$  is a flux estimate across the two deepest measurement layers.
- $F_{101}$  is a flux estimate across the shallowest and deepest measurement layers.

For  $F_{110}$ ,  $F_{011}$ , and  $F_{101}$ , the diffusivity used in Fick's Law is always at the deeper measurement layer. When used as a surface flux estimate we assume CO<sub>2</sub> remains constant above this flux depth. Uncertainty in all  $F_{ijk}$  values was quantified using quadrature (Taylor, 2022). These computed fluxes could provide the basis for additional soil flux estimates. For example, Tang et al. (2005) estimated surface flux by linearly extrapolating  $F_{110}$  and  $F_{011}$  to the soil surface.

### 3.3 Post processing evaluation

Following collection of field measurements and calculation of the soil fluxes from `neonSoilFlux` package, we compared measured  $F_S$  based on closed-dynamic chamber measurements with the LI-COR instruments to a given soil flux calculation from `neonSoilFlux` for each site and flux computation method and quantified the relationship statistically ( $R^2$ ). Finally, for a half-hourly interval we also computed a *post hoc* diffusivity ( $D_a$ ) using the LI-COR flux along with the CO<sub>2</sub> surface gradient reported by NEON using the measurement levels closest to the surface.

Table 2: Summary of measured soil characteristics and flux results from field measurements across six NEON sites using a LI-COR 6800 (LI-870/8250 measurements omitted to enable direct comparability) via the closed-dynamic chamber method. Numeric values for soil CO<sub>2</sub> flux, soil temperature, and volumetric soil water content (VSWC) are the mean and standard deviation of field measurements at each site.

Site	Flux μmol m <sup>-2</sup> s <sup>-1</sup>	Soil temp °C	VSWC cm <sup>3</sup> cm <sup>-3</sup>	n
UNDE	2.55 ± 0.26	14.33 ± 0.77	0.33 ± 0.02	61
WOOD	3.02 ± 0.4	16.01 ± 1.54	0.28 ± 0.01	53
WREF	3.62 ± 0.3	15.34 ± 1.76	0.27 ± 0.06	21
KONZ	6.35 ± 0.97	27.28 ± 4.14	0.37 ± 0.01	44
SJER	0.94 ± 0.02	41.68 ± 11.22	0.01 ± 0.01	32
SRER	0.72 ± 0.09	47.64 ± 7.46	0.04 ± 0.01	32

## 4 Results

### 4.1 Concordance between modelled and measured soil CO<sub>2</sub> flux

The sites we visited ranged substantially in both their annual average temperature and precipitation as well as their biome type (Table 2). These differences also influenced the wide range of observed flux rates across sites.

The timeseries of the measured fluxes from the LI-COR 6800 and 870/8250 were compared to modeled soil fluxes from the `neonSoilFlux` R package (Figure 4). We also assessed year-long estimated flux time series and compared those to field measurements made at each site (Figure 5). Results are reported in local time. Where applicable, sites are displayed from left to right by increasing soil temperature (Table 1). Positive values of the flux indicate that there is a flux moving towards the surface. Overall, with the exception of SRER (discussed later) the computed fluxes determined using a variety of plausible methods spanned the field-measured fluxes, but the specific flux-gradient method that best approximated field measurements varied by site.

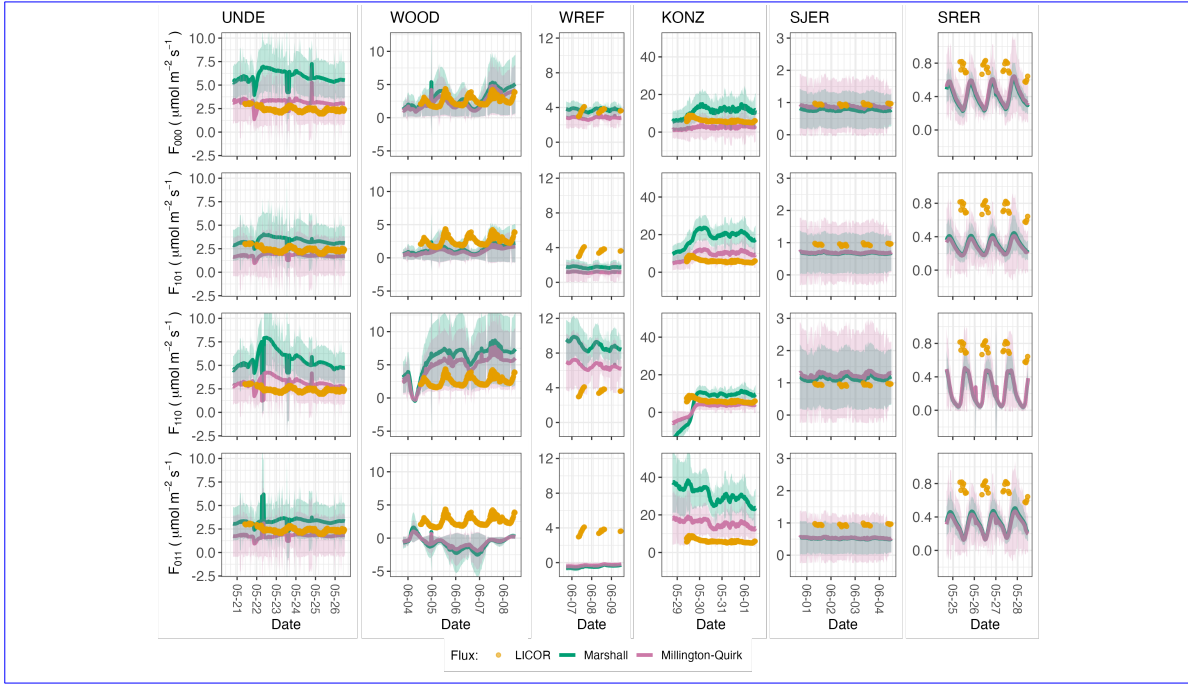


Figure 4: Timeseries of soil surface flux ( $F_S$ ) from field-measured (yellow lines) and modeled soil fluxes (green or purple lines) by the `neonSoilFlux` R package. Fluxes from the `neonSoilFlux` R package are separated by the diffusivity model used (Millington-Quirk or Marshall, Section 3.2.2). Individual vertical axis labels in the first column represent the measurement levels where the flux-gradient approach is applied (Section 3.2.3). Ribbons for modeled soil fluxes represent approximately  $\pm 1$  standard deviation. Results are reported in local time. WREF, SJER, and SRER were sampled in 2022, and UNDE, WOOD, and KONZ were sampled in 2024. Sites (columns) are arranged from left to right in terms of increasing mean annual temperature.

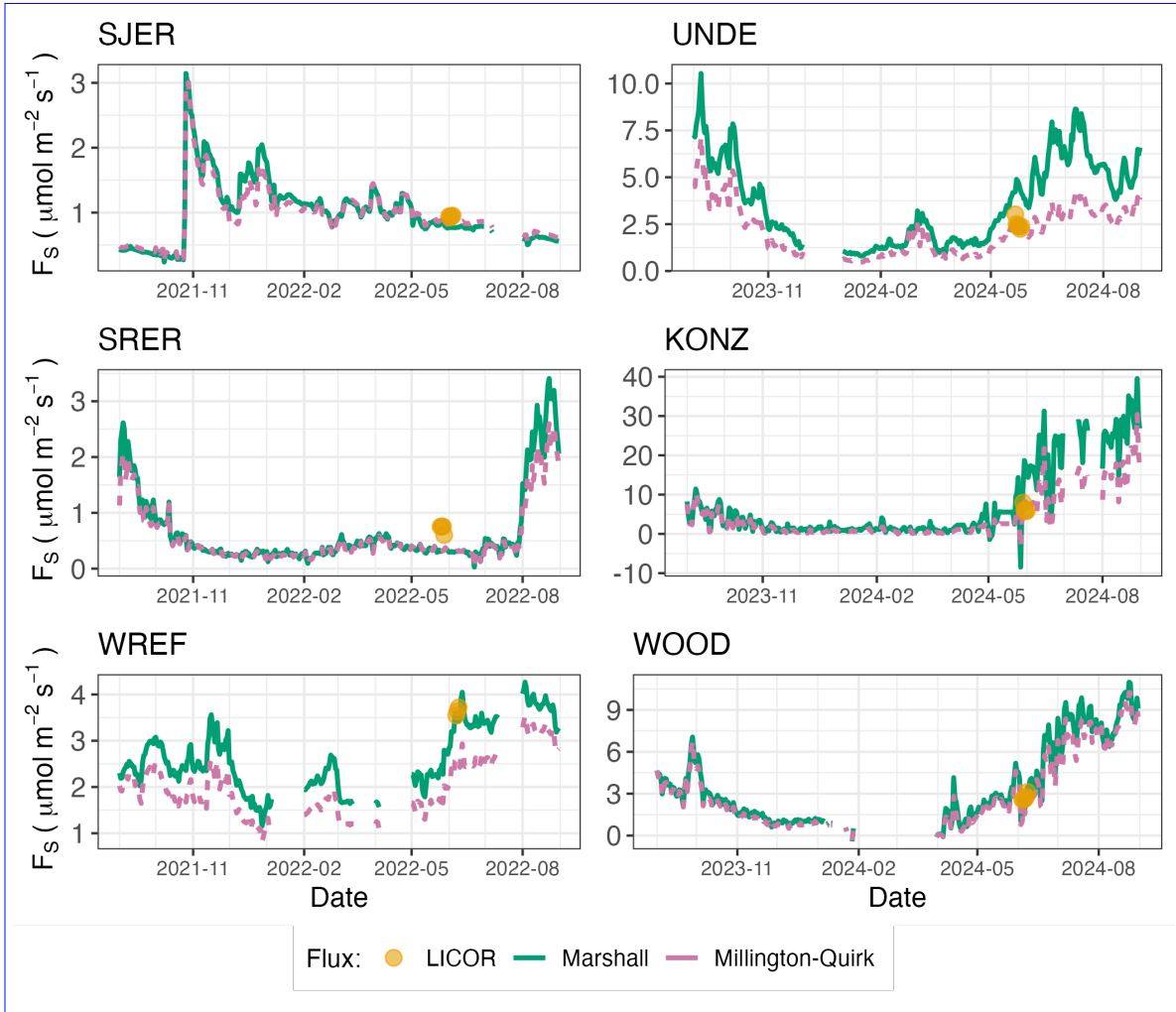


Figure 5: Timeseries of both daily-averaged field  $F_S$  (yellow circles) and daily ensemble averaged soil fluxes (average of  $F_{000}$ ,  $F_{101}$ ,  $F_{011}$ ,  $F_{110}$ , Section 3.2.3) by the `neonSoilFlux` R package, separated by the diffusivity model used (green or purple lines, Millington-Quirk or Marshall, Section 3.2.2).

337 We calculated a statistical relationship between the various estimates of soil flux computed by  
338 `neonSoilFlux` and the field-measured fluxes within daily interval periods. Statistics for these  
339 comparisons are reported in Figure 6, which also shows how these fall relative to a 1:1 line.

340 **4.2 Effects of method choice on diffusivity estimates**

341 In ~~four-of-one of the~~ six field sites, the *post hoc*  $D_a$  estimate fell roughly between the two  
342 diffusion estimation methods; ~~however this was less the case in the two~~. At UNDE, WOOD,  
WREF, and SJER, the median field estimate of diffusivity was lower than both of the other  
methods. At the driest sites, SJER and SRER (Table 1), ~~where the~~ the median field estimate  
345 of diffusivity was ~~either lower or~~ higher than both of the other methods and values showed a  
346 large amount of variation (Figure 7).

347 **5 Discussion**

348 This study presents a unified data science workflow to efficiently process automated measure-  
349 ments of belowground soil CO<sub>2</sub> concentrations, soil water content, and soil temperature to  
350 infer estimates of soil surface CO<sub>2</sub> effluxes through application of Fick's Law (Equation 4).  
351 Our core goals in this study were: (1) to generate estimates of soil flux from continuous soil  
352 sensor data at terrestrial NEON sites using the flux-gradient method and then (2) to compare  
353 those estimates to field-measured fluxes based on the closed chamber approach at six NEON  
354 focal sites. We discuss our progress toward these core goals through (1) an overall evaluation  
355 of the flux-gradient approach (and uncertainty calculation) and (2) site-specific evaluation of  
356 differences in estimated vs measured fluxes.

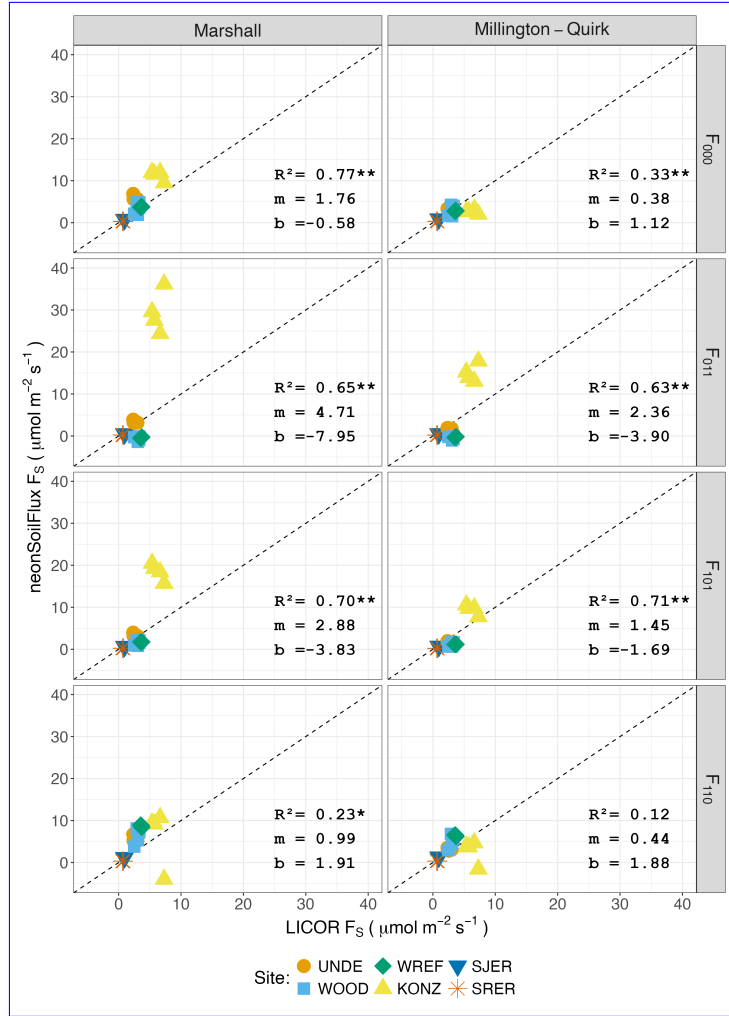


Figure 6: Statistical comparison between measured fluxes at each NEON site with fluxes reported by `neonSoilFlux` with the different flux calculation approaches and diffusivity calculations applied. Points are daily averages and LICOR  $F_S$  values are from the 6800 instrument only, for consistency. The dotted line represents a 1:1 relationship, and the reported  $R^2$  quantifies the relationship between field-measured and `neonSoilFlux` estimated fluxes. \* = significance at the 5% level, \*\* = significance at the 1% level. The [slope \( \$m\$ \) and intercept \( \$b\$ \) of the linear regression between measured and modeled fluxes are also reported](#). The low-value outlier from KONZ in the  $F_{110}$  Marshall plot is an example of the effect of inverted CO<sub>2</sub> gradients causing an estimated flux to be negative, bringing down the daily mean, which later resolved as the soils dried back out.

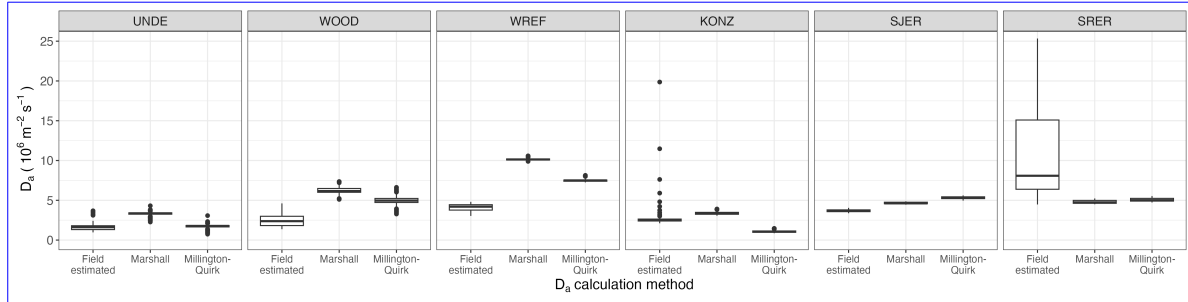


Figure 7: Distribution of diffusivity ( $D_a$ ) at each study site. Values of  $D_a$  were provided by the `neonSoilFlux` package, computed from the Millington-Quirk or Marshall models (Section 3.2.2). A post-hoc estimate of diffusivity (labeled as “Field estimated”) was computed through the field measured flux (Figure 4), divided by the CO<sub>2</sub> gradient from the measurement levels closest to the soil surface, as reported by NEON. We only used  $F_S$  measured by the LICOR 6800 at all sites to standardize comparisons. Some outliers ( $n = 1$  from the field estimated values at KONZ and  $n = 6$  from field estimated values at SRER) are excluded from the plot to allow better comparative visualization across sites.

### 357 5.1 General evaluation of flux-gradient approach

358 Key assumptions of the flux-gradient approach are that CO<sub>2</sub> concentrations increase throughout  
 359 the soil profile such that the highest concentrations are observed in the deepest layers. Addition-  
 360 ally, field flux measurements should correlate with  $F_{000}$  because they represent surface fluxes.  
 361 Periods where this gradient condition are not met generally are connected to processes that occur  
 362 during soil wetting events, where more shallow soil layers produce higher concentrations of CO<sub>2</sub>  
 363 due to microbial respiration pulses following rewetting. This effect is likely to be largest at sites  
 364 with rich organic soils (e.g. KONZ). Based on this reasoning, in these types of situations we would  
 365 *a priori* expect  $F_{011}$  (deepest layers)  $\leq F_{101} \leq F_{110}$  (shallow layers)  $\leq F_{000}$  (all layers) be-  
 366 cause the previous flux estimates rely primarily on CO<sub>2</sub> concentrations at deeper depths, and  
 367 could miss high concentrations of CO<sub>2</sub> produced in shallower layers.

368 When modeling soil respiration, typically a non-linear response function that also considers soil  
 369 type is used (Bouma & Bryla, 2000; Yan et al., 2016, 2018). For the `neonSoilFlux` package,

370 soil type is connected to the measurement of bulk density, which was characterized at each  
371 NEON site. This bulk density estimate is based on replicate samples collected from the site  
372 megapit at a subset of soil horizons, with an estimated uncertainty of  $\pm 5\%$  ([National Ecological](#)  
373 [Observatory Network \(NEON\)](#)[NEON](#), 2024c). Coarse fragment estimates also have very large  
374 uncertainties, but because the volume fraction tends to be low in surface soils it is unlikely to  
375 contribute much additional flux uncertainty.

376 Our results suggest that the most important way to improve reliability of the flux estimate is  
377 to reduce the usage of gap-filled data. The current approach to gap filling in `neonSoilFlux`  
378 uses monthly mean data to gap fill—this approach decreases the ability of the estimate to be  
379 responsive to short-term pulses that occur with rapid weather shifts. [Four sites \(KONZ, SRER,](#)  
380 [WREF, and UNDE\)](#) [All sites](#) had more than 75% of half-hourly periods with no-gap filled  
381 measurements (Figure S1, Supplementary Information). [Two sites \(SJER and WOOD\) had](#)  
382 [more than 75% of half-hourly intervals with just one](#) [At five out of six sites \(all except SRER\),](#)  
383 [we used at least some](#) gap-filled [measurement](#). [The large uncertainty evident in Figure 4 for](#)  
384 [estimates from WOOD and SJER are thus due in part to the gap-filling used in these sites](#)  
385 [\(Figure S1\).](#) While we did not need to use gap-filled measurements to compute the flux at  
386 [of Soil Water Content \(SWC\).](#) At WREF, field data collection occurred following a severe  
387 rainstorm, with soils at the beginning of the sampling week near their water holding capacity.  
388 [which can influence the soil moisture sensor accuracy](#). In general, we recommend that whenever  
389 possible, knowledge of local field conditions should influence analysis decisions in addition to  
390 any QA filtering protocols in the `neonSoilFlux` package.

391 We recognize that this gap-filling approach may lead to gap-filled values that are quite different  
392 from the actual values, such as an underestimate of soil moisture following rain events. Further  
393 extensions of the gap filling method could use more sophisticated gap-filling routines, similar to  
394 what is used for net ecosystem carbon exchange (Falge et al., 2001; Liu et al., 2023; Mariethoz

et al., 2015; Moffat et al., 2007; Zhang et al., 2023). Additionally, since the deepest temperature and soil moisture sensors are located below the deepest CO<sub>2</sub> sensors at NEON sites, it is possible that excluding these deeper layers from consideration prior to analysis would lead to a reduced need for gap filling. Future iterations of the `neonSoilFlux` package may incorporate this as an option. The current gap-filling routine provides a consistent approach that can be applied to each data stream, but further work may explore alternative gap-filling approaches.

## 5.2 Evaluation of flux-gradient approach at each site

Derived results from the `neonSoilFlux` package have patterns that are broadly consistent with those directly measured in the field (Figure 4 and Figure 5), even though statistical comparisons between the field-measured and `neonSoilFlux` values were quite variable (e.g.  $R^2$  ranging from ~~0.04 to 0.81~~<sup>0.12 to 0.77</sup>; Figure 6). One advantage of the `neonSoilFlux` package is its ability to calculate fluxes across different soil depths (Figure 3), which allows for additional site-specific customization. We believe the package can provide a useful baseline estimate of soil fluxes that can always be complemented through additional field measurements.

The six locations studied provide a range of case studies that suggest different considerations may apply to different sites when applying the flux-gradient method. For example, the Santa Rita Experimental Range (SRER) is a desert site characterized by sandy soil, which also was the location of the highest field soil temperatures that we observed (Table 2). At SRER the flux across the top two layers ( $F_{110}$ ) produced a pattern of soil flux most consistent with the observed field data. The remaining methods  $F_{101}$ ,  $F_{011}$ , or  $F_{000}$  are derived from information taken from the deepest layer, which seems to have been decoupled from the surface layers both in terms of temperature and CO<sub>2</sub> concentration. This may be a general circumstance where there are large diurnal temperature extremes that rapidly change during the course of a day

418 and overnight, leading to lags in the timing of when temperature increases propagate down to  
419 deeper soil layers.

420 Immediately prior to our visit to Konza Prairie (KONZ), that site that experienced a significant  
421 rain event that led to wet soils that gradually dried out over the course of our time there.  
422 This pulse of precipitation increased the soil CO<sub>2</sub> concentration at the top layer above the  
423 concentrations in lower layers, leading to negative estimated flux values at the start of the field  
424 sampling period. In this case it was only when the soil began to return to a baseline level that  
425 the assumptions of the flux-gradient method were again met.

426 Both of the previous cases also provide context for the variable statistical comparisons between  
427 field-measured soil fluxes and `neonSoilFlux` outputs (Figure 6). When considering systematic  
428 deployment of this method across a measurement network, there are a number of independent  
429 challenges that require careful consideration. There are clear tradeoffs between (1) accuracy of  
430 modeled fluxes (defined here as closeness to field-measured  $F_S$  and the uncertainty reduction  
431 factor  $\epsilon$ ), (2) precision (which could be defined by the signal to noise ratio), and (3) the choice of  
432 the diffusivity model (Section 3.2.2) or flux computation method (Section 3.2.3). ~~A sensitivity~~  
433 ~~analysis~~ We performed a sensitivity analysis to compare the impact of these factors (Figure S2,  
434 Supplemental Information) ~~found that flux output uncertainty was dominated by measurement~~  
435 ~~uncertainty ( $T_S$ ,  $P$ , SWC, or CO<sub>2</sub>) rather than by the diffusivity method used to compute soil~~  
436 ~~flux. Notably, the  $F_{110}$  method was least sensitive to measurement uncertainty likely because~~  
437 ~~it best aligns with the surface chamber measurement assumptions.~~ .

438 Finally, comparing the effects of different diffusivity estimation methods on the match between  
439 modeled and measured fluxes (Figure 5) highlights the sensitivity of  $F_{ijk}$  to diffusivity. The  
440 comparison between diffusivity estimates compared to field estimated diffusivity (Figure 7)  
441 demonstrates that site parameters can dictate which measure of diffusivity is most likely to be  
442 accurate in a given environmental context. Site-specific differences are largely a reflection of

443 differences in soil moisture across the sites (Table 1), as not all diffusivity estimation methods  
444 incorporate soil moisture equivalently. While we here have compares two approaches to calculate  
445 diffusivity (the Millington-Quirk and Marshall models), it may be valuable to evaluate other  
446 diffusivity models (e.g. the Moldrup model; Moldrup et al. (1999)) as well. Ultimately the  
447 choice of a particular diffusivity model could be determined based on knowledge of site-specific  
448 evaluations or a set of these models could be used to generate a model ensemble average as a  
449 means to trade precision for a more general approach.

### 450 **5.3 Recommendations for future method development**

451 The `neonSoilFlux` package provides several approaches to estimate soil flux using the gradient  
452 method. We believe these approaches enable the software to be used across a range of site-  
453 specific assumptions (Maier & Schack-Kirchner, 2014). We note, however, that this choice  
454 can have a determinative approach on the calculated values. Ensemble averaging approaches  
455 (Elshall et al., 2018; Raftery et al., 2005) may be one way to address this problem if the goal  
456 is to calculate fluxes using the same method at a diverse range of different sites. Two other  
457 ideas would be to apply machine learning algorithms ([e.g. `e.g.`](#) random forest) to generate a  
458 single flux estimate across diverse sites, or using co-located estimates of net ecosystem carbon  
459 exchange from eddy-flux towers to further constrain results or to assess soil flux results for  
460 plausibility (Phillips et al., 2017).

461 These challenges notwithstanding, the method used here and made available in the  
462 `neonSoilFlux` R package has the potential to produce nearly continuous estimates of flux  
463 across all terrestrial NEON sites. These estimates are a significant improvement on available  
464 approaches to constrain the portion of ecosystem respiration attributable to the soil. This, in  
465 turn, also aids in our ability to understand the soil contribution to the net ecosystem flux  
466 measured at these sites using the co-located eddy flux towers.

<sup>467</sup> **6 Conclusions**

<sup>468</sup> We used the R package `neonSoilFlux` to estimate soil CO<sub>2</sub> fluxes with the flux-gradient method  
<sup>469</sup> using data from buried soil sensors at NEON terrestrial sites. We compared the predicted  
<sup>470</sup> fluxes to those measured directly using a field-based closed chamber approach. Soil fluxes  
<sup>471</sup> from `neonSoilFlux` were broadly effective at producing estimates of flux comparable to those  
<sup>472</sup> measured in the field using a chamber-based technique. However `neonSoilFlux` outputs are  
<sup>473</sup> quite sensitive to a number of issues, including: missing data (and thus gap-filling of input  
<sup>474</sup> measurement datasets), the selection of soil depths used to best calculate the gradient (which  
<sup>475</sup> may vary between sites), and finally the choice of method used for estimating soil diffusivity.  
<sup>476</sup> The flexibility of the `neonSoilFlux` package allows the user to evaluate each of these issues  
<sup>477</sup> with site-specific knowledge and contexts. Future refinements and subsequent validation of  
<sup>478</sup> `neonSoilFlux` outputs will feed forward into evaluating soil carbon fluxes broader spatial scales  
<sup>479</sup> to enhance understanding of the ways in which soils across diverse ecosystems are responding  
<sup>480</sup> to a changing climate.

<sup>481</sup> **Sources Cited**

- <sup>482</sup> Ayres, E., Reichle, R. H., Colliander, A., Cosh, M. H., & Smith, L. (2024). Validation of  
<sup>483</sup> Remotely Sensed and Modeled Soil Moisture at Forested and Unforested NEON Sites.  
<sup>484</sup> *IEEE Journal of Selected Topics in Applied Earth Observations and Remote Sensing*, 17,  
<sup>485</sup> 14248–14264. <https://doi.org/10.1109/JSTARS.2024.3430928>
- <sup>486</sup> Baldocchi, D. (2014). Measuring fluxes of trace gases and energy between ecosystems and the  
<sup>487</sup> atmosphere - the state and future of the eddy covariance method. *Global Change Biology*,  
<sup>488</sup> 20(12), 3600–3609. <https://doi.org/10.1111/gcb.12649>

- 489 Berenbaum, M. R., Carpenter, S. R., Hampton, S. E., Running, S. W., & Stanzione, D. C.  
490 (2015). *Report from the NSF BIO Advisory Committee Subcommittee on NEON Scope*  
491 *Impacts*.
- 492 Bond-Lamberty, B. (2018). New Techniques and Data for Understanding the Global Soil  
493 Respiration Flux. *Earth's Future*, 6(9), 1176–1180. <https://doi.org/10.1029/2018EF000866>
- 494 Bond-Lamberty, B., Ballantyne, A., Berryman, E., Fluet-Chouinard, E., Jian, J., Morris, K.  
495 A., Rey, A., & Vargas, R. (2024). Twenty Years of Progress, Challenges, and Opportuni-  
496 ties in Measuring and Understanding Soil Respiration. *Journal of Geophysical Research: Bio-geosciences*, 129(2), e2023JG007637. <https://doi.org/10.1029/2023JG007637>
- 497 Bond-Lamberty, B., Christianson, D. S., Malhotra, A., Pennington, S. C., Sihi, D., AghaK-  
498 ouchak, A., Anjileli, H., Altaf Arain, M., Armesto, J. J., Ashraf, S., Ataka, M., Baldocchi,  
499 D., Andrew Black, T., Buchmann, N., Carbone, M. S., Chang, S.-C., Crill, P., Curtis, P.  
500 S., Davidson, E. A., ... Zou, J. (2020). COSORE: A community database for continuous  
501 soil respiration and other soil-atmosphere greenhouse gas flux data. *Global Change Biology*,  
502 26(12), 7268–7283. <https://doi.org/10.1111/gcb.15353>
- 503 Bond-Lamberty, B., & Thomson, A. (2010). A global database of soil respiration data.  
504 *Biogeosciences*, 7(6), 1915–1926. <https://doi.org/10.5194/bg-7-1915-2010>
- 505 Bond-Lamberty, B., Wang, C., & Gower, S. T. (2004). A global relationship between the  
506 heterotrophic and autotrophic components of soil respiration? *Global Change Biology*,  
507 10(10), 1756–1766. <https://doi.org/10.1111/j.1365-2486.2004.00816.x>
- 508 Bouma, T. J., & Bryla, D. R. (2000). On the assessment of root and soil respiration for soils of  
509 different textures: Interactions with soil moisture contents and soil CO<sub>2</sub> concentrations.  
510 *Plant and Soil*, 227(1), 215–221. <https://doi.org/10.1023/A:1026502414977>
- 511 Chen, H., & Tian, H.-Q. (2005). Does a General Temperature-Dependent Q10 Model of Soil  
512 Respiration Exist at Biome and Global Scale? *Journal of Integrative Plant Biology*, 47(11),  
513 1288–1302. <https://doi.org/10.1111/j.1744-7909.2005.00211.x>

- 515 Davidson, E. A., Janssens, I. A., & Luo, Y. (2006). On the variability of respiration in  
516 terrestrial ecosystems: Moving beyond Q10. *Global Change Biology*, 12, 154–164. <https://doi.org/10.1111/j.1365-2486.2005.01065.x>
- 517
- 518 Desai, A. R., Murphy, B. A., Wiesner, S., Thom, J., Butterworth, B. J., Koupaei-Abyazani, N.,  
519 Muttaqin, A., Paleri, S., Talib, A., Turner, J., Mineau, J., Merrelli, A., Stoy, P., & Davis,  
520 K. (2022). Drivers of Decadal Carbon Fluxes Across Temperate Ecosystems. *Journal of*  
521 *Geophysical Research: Biogeosciences*, 127(12), e2022JG007014. <https://doi.org/10.1029/2022JG007014>
- 522
- 523 Efron, B., & Tibshirani, R. J. (1994). *An Introduction to the Bootstrap*. Chapman and  
524 Hall/CRC. <https://doi.org/10.1201/9780429246593>
- 525 Elshall, A. S., Ye, M., Pei, Y., Zhang, F., Niu, G.-Y., & Barron-Gafford, G. A. (2018). Relative  
526 model score: A scoring rule for evaluating ensemble simulations with application to microbial  
527 soil respiration modeling. *Stochastic Environmental Research and Risk Assessment*, 32(10),  
528 2809–2819. <https://doi.org/10.1007/s00477-018-1592-3>
- 529 Falge, E., Baldocchi, D., Olson, R., Anthoni, P., Aubinet, M., Bernhofer, C., Burba, G.,  
530 Ceulemans, R., Clement, R., Dolman, H., Granier, A., Gross, P., Grünwald, T., Hollinger,  
531 D., Jensen, N.-O., Katul, G., Keronen, P., Kowalski, A., Lai, C. T., ... Wofsy, S. (2001).  
532 Gap filling strategies for defensible annual sums of net ecosystem exchange. *Agricultural*  
533 *and Forest Meteorology*, 107(1), 43–69. [https://doi.org/10.1016/S0168-1923\(00\)00225-2](https://doi.org/10.1016/S0168-1923(00)00225-2)
- 534 Farrance, I., & Frenkel, R. (2012). Uncertainty of Measurement: A Review of the Rules  
535 for Calculating Uncertainty Components through Functional Relationships. *The Clinical*  
536 *Biochemist Reviews*, 33(2), 49–75.
- 537 Friedlingstein, P., O’Sullivan, M., Jones, M. W., Andrew, R. M., Hauck, J., Landschützer,  
538 P., Le Quéré, C., Li, H., Luijkx, I. T., Olsen, A., Peters, G. P., Peters, W., Pongratz, J.,  
539 Schwingshackl, C., Sitch, S., Canadell, J. G., Ciais, P., Jackson, R. B., Alin, S. R., ...  
540 Zeng, J. (2025). Global Carbon Budget 2024. *Earth System Science Data*, 17(3), 965–1039.

- 541           <https://doi.org/10.5194/essd-17-965-2025>
- 542     Hamdi, S., Moyano, F., Sall, S., Bernoux, M., & Chevallier, T. (2013). Synthesis analysis  
543       of the temperature sensitivity of soil respiration from laboratory studies in relation to  
544       incubation methods and soil conditions. *Soil Biology and Biochemistry*, 58, 115–126.  
545           <https://doi.org/10.1016/j.soilbio.2012.11.012>
- 546     Jackson, R. B., Lajtha, K., Crow, S. E., Hugelius, G., Kramer, M. G., & Piñeiro, G. (2017).  
547       The Ecology of Soil Carbon: Pools, Vulnerabilities, and Biotic and Abiotic Controls.  
548       *Annual Review of Ecology, Evolution and Systematics*, 48(Volume 48, 2017), 419–445.  
549           <https://doi.org/10.1146/annurev-ecolsys-112414-054234>
- 550     Jian, J., Bailey, V., Dorheim, K., Konings, A. G., Hao, D., Shiklomanov, A. N., Snyder,  
551       A., Steele, M., Teramoto, M., Vargas, R., & Bond-Lamberty, B. (2022). Historically  
552       inconsistent productivity and respiration fluxes in the global terrestrial carbon cycle. *Nature  
553       Communications*, 13(1), 1733. <https://doi.org/10.1038/s41467-022-29391-5>
- 554     Jian, J., Vargas, R., Anderson-Teixeira, K., Stell, E., Herrmann, V., Horn, M., Kholod, N.,  
555       Manzon, J., Marchesi, R., Paredes, D., & Bond-Lamberty, B. (2021). A restructured and  
556       updated global soil respiration database (SRDB-V5). *Earth System Science Data*, 13(2),  
557       255–267. <https://doi.org/10.5194/essd-13-255-2021>
- 558     Jiang, J., Feng, L., Hu, J., Liu, H., Zhu, C., Chen, B., & Chen, T. (2024). Global soil  
559       respiration predictions with associated uncertainties from different spatio-temporal data  
560       subsets. *Ecological Informatics*, 82, 102777. <https://doi.org/10.1016/j.ecoinf.2024.102777>
- 561     Jobbágy, E. G., & Jackson, R. B. (2000). The Vertical Distribution of Soil Organic Carbon  
562       and its Relation to Climate and Vegetation. *Ecological Applications*, 10(2), 423–436.  
563           [https://doi.org/10.1890/1051-0761\(2000\)010%5B0423:TVDOSO%5D2.0.CO;2](https://doi.org/10.1890/1051-0761(2000)010%5B0423:TVDOSO%5D2.0.CO;2)
- 564     Jurasinski, G., Koebisch, F., Guenther, A., & Beetz, S. (2022). *Flux: Flux Rate Calculation  
565       from Dynamic Closed Chamber Measurements.*
- 566     Liu, K., Li, X., Wang, S., & Zhang, H. (2023). A robust gap-filling approach for European

- 567 Space Agency Climate Change Initiative (ESA CCI) soil moisture integrating satellite  
568 observations, model-driven knowledge, and spatiotemporal machine learning. *Hydrology*  
569 and *Earth System Sciences*, 27(2), 577–598. <https://doi.org/10.5194/hess-27-577-2023>
- 570 Lunch, C., Laney, C., Mietkiewicz, N., Sokol, E., Cawley, K., & NEON (National Ecological  
571 Observatory Network). (Network), N. (National. E. Q.). (2025). *neonUtilities: Utilities for*  
572 *working Working with NEON dataData*.
- 573 Luo, Y., Ogle, K., Tucker, C., Fei, S., Gao, C., LaDeau, S., Clark, J. S., & Schimel, D. S. (2011).  
574 Ecological forecasting and data assimilation in a data-rich era. *Ecological Applications*,  
575 21(5), 1429–1442. <https://doi.org/10.1890/09-1275.1>
- 576 Maier, M., & Schack-Kirchner, H. (2014). Using the gradient method to determine soil gas  
577 flux: A review. *Agricultural and Forest Meteorology*, 192–193, 78–95. <https://doi.org/10.1016/j.agrformet.2014.03.006>
- 579 Mariethoz, G., Linde, N., Jougnot, D., & Rezaee, H. (2015). Feature-preserving interpolation  
580 and filtering of environmental time series. *Environmental Modelling & Software*, 72, 71–76.  
581 <https://doi.org/10.1016/j.envsoft.2015.07.001>
- 582 Marshall, T. J. (1959). The Diffusion of Gases Through Porous Media. *Journal of Soil Science*,  
583 10(1), 79–82. <https://doi.org/10.1111/j.1365-2389.1959.tb00667.x>
- 584 Millington, R. J., & Shearer, R. C. (1971). Diffusion in aggregated porous media. *Soil Science*,  
585 111(6), 372–378.
- 586 Moffat, A. M., Papale, D., Reichstein, M., Hollinger, D. Y., Richardson, A. D., Barr, A. G.,  
587 Beckstein, C., Braswell, B. H., Churkina, G., Desai, A. R., Falge, E., Gove, J. H., Heimann,  
588 M., Hui, D., Jarvis, A. J., Kattge, J., Noormets, A., & Stauch, V. J. (2007). Comprehensive  
589 comparison of gap-filling techniques for eddy covariance net carbon fluxes. *Agricultural and*  
590 *Forest Meteorology*, 147(3), 209–232. <https://doi.org/10.1016/j.agrformet.2007.08.011>
- 591 Moldrup, P., Olesen, T., Yamaguchi, T., Schjønning, P., & Rolston, D. E. (1999). Modeling  
592 diffusion and reaction in soils: 9. The Buckingham-Burdine-Campbell equation for gas

- 593 diffusivity in undisturbed soil. *Soil Science*, 164(2), 75.
- 594 ~~National Ecological Observatory Network (NEON)~~NEON. (2024a). *Barometric pres-*  
595 *sure (DP1.00004.001)*. National Ecological Observatory Network (NEON). <https://doi.org/10.48443/RT4V-KZ04>
- 596 ~~National Ecological Observatory Network (NEON)~~NEON. (2024b). *Soil CO<sub>2</sub> concentration*  
597 *(DP1.00095.001)*. National Ecological Observatory Network (NEON). <https://doi.org/10.48443/E7GR-6G94>
- 598 ~~National Ecological Observatory Network (NEON)~~NEON. (2024c). *Soil physical and chemical*  
599 *properties, Megapit (DP1.00096.001)*. National Ecological Observatory Network (NEON).  
600 <https://doi.org/10.48443/S6ND-Q840>
- 601 ~~National Ecological Observatory Network (NEON)~~NEON. (2024d). *Soil tempera-*  
602 *ture (DP1.00041.001)*. National Ecological Observatory Network (NEON). <https://doi.org/10.48443/Q24X-PW21>
- 603 ~~National Ecological Observatory Network (NEON)~~NEON. (2024e). *Soil water content and*  
604 *water salinity (DP1.00094.001)*. National Ecological Observatory Network (NEON). <https://doi.org/10.48443/A8VY-Y813>
- 605 Norman, J. M., Kucharik, C. J., Gower, S. T., Baldocchi, D. D., Crill, P. M., Rayment,  
606 M., Savage, K., & Striegl, R. G. (1997). A comparison of six methods for measuring  
607 soil-surface carbon dioxide fluxes. *Journal of Geophysical Research: Atmospheres*, 102(D24),  
608 28771–28777. <https://doi.org/10.1029/97JD01440>
- 609 Pedersen, A. R. (2024). *HMR: Flux Estimation with Static Chamber Data*.
- 610 Phillips, C. L., Bond-Lamberty, B., Desai, A. R., Lavoie, M., Risk, D., Tang, J., Todd-Brown,  
611 K., & Vargas, R. (2017). The value of soil respiration measurements for interpreting and  
612 modeling terrestrial carbon cycling. *Plant and Soil*, 413(1), 1–25. <https://doi.org/10.1007/s11104-016-3084-x>
- 613 Raftery, A. E., Gneiting, T., Balabdaoui, F., & Polakowski, M. (2005). *Using Bayesian Model*

- 619      *Averaging to Calibrate Forecast Ensembles.* <https://doi.org/10.1175/MWR2906.1>
- 620    Rheault, K., Christiansen, J. R., & Larsen, K. S. (2024). goFlux: A user-friendly way to  
621       calculate GHG fluxes yourself, regardless of user experience. *Journal of Open Source*  
622       *Software*, 9(96), 6393. <https://doi.org/10.21105/joss.06393>
- 623    Sallam, A., Jury, W. A., & Letey, J. (1984). Measurement of Gas Diffusion Coefficient under  
624       Relatively Low Air-filled Porosity. *Soil Science Society of America Journal*, 48(1), 3–6.  
625       <https://doi.org/10.2136/sssaj1984.03615995004800010001x>
- 626    Shao, J., Zhou, X., Luo, Y., Li, B., Aurela, M., Billesbach, D., Blanken, P. D., Bracho, R.,  
627       Chen, J., Fischer, M., Fu, Y., Gu, L., Han, S., He, Y., Kolb, T., Li, Y., Nagy, Z., Niu, S.,  
628       Oechel, W. C., ... Zhang, J. (2015). Biotic and climatic controls on interannual variability  
629       in carbon fluxes across terrestrial ecosystems. *Agricultural and Forest Meteorology*, 205,  
630       11–22. <https://doi.org/10.1016/j.agrformet.2015.02.007>
- 631    Shao, P., Zeng, X., Moore, D. J. P., & Zeng, X. (2013). Soil microbial respiration from  
632       observations and Earth System Models. *Environmental Research Letters*, 8(3), 034034.  
633       <https://doi.org/10.1088/1748-9326/8/3/034034>
- 634    Sihi, D., Gerber, S., Inglett, P. W., & Inglett, K. S. (2016). Comparing models of microbial–  
635       substrate interactions and their response to warming. *Biogeosciences*, 13(6), 1733–1752.  
636       <https://doi.org/10.5194/bg-13-1733-2016>
- 637    Tang, J., Baldocchi, D. D., Qi, Y., & Xu, L. (2003). Assessing soil CO<sub>2</sub> efflux using continuous  
638       measurements of CO<sub>2</sub> profiles in soils with small solid-state sensors. *Agricultural and Forest*  
639       *Meteorology*, 118(3), 207–220. [https://doi.org/10.1016/S0168-1923\(03\)00112-6](https://doi.org/10.1016/S0168-1923(03)00112-6)
- 640    Tang, J., Misson, L., Gershenson, A., Cheng, W., & Goldstein, A. H. (2005). Continuous  
641       measurements of soil respiration with and without roots in a ponderosa pine plantation  
642       in the Sierra Nevada Mountains. *Agricultural and Forest Meteorology*, 132(3), 212–227.  
643       <https://doi.org/10.1016/j.agrformet.2005.07.011>
- 644    Taylor, J. R. (2022). *An Introduction to Error Analysis: The Study of Uncertainties in Physical*

- 645 *Measurements*, Third Edition (3rd ed.). University Science Press.
- 646 Wilson, S. J., Bond-Lamberty, B., Noyce, G., Bittencourt Peixoto, R., & Megonigal,  
647 J. P. (2024). Fluxfinder: An R Package for Reproducible Calculation and Initial  
648 Processing of Greenhouse Gas Fluxes From Static Chamber Measurements. *Journal of*  
649 *Geophysical Research: Biogeosciences*, 129(11), e2024JG008208. <https://doi.org/10.1029/2024JG008208>
- 650
- 651 Yan, Z., Bond-Lamberty, B., Todd-Brown, K. E., Bailey, V. L., Li, S., Liu, C., & Liu, C. (2018).  
652 A moisture function of soil heterotrophic respiration that incorporates microscale processes.  
653 *Nature Communications*, 9(1), 2562. <https://doi.org/10.1038/s41467-018-04971-6>
- 654 Yan, Z., Liu, C., Todd-Brown, K. E., Liu, Y., Bond-Lamberty, B., & Bailey, V. L. (2016).  
655 Pore-scale investigation on the response of heterotrophic respiration to moisture conditions  
656 in heterogeneous soils. *Biogeochemistry*, 131(1), 121–134. <https://doi.org/10.1007/s10533-016-0270-0>
- 657
- 658 Zhang, R., Kim, S., Kim, H., Fang, B., Sharma, A., & Lakshmi, V. (2023). Temporal Gap-Filling  
659 of 12-Hourly SMAP Soil Moisture Over the CONUS Using Water Balance Budgeting. *Water  
660 Resources Research*, 59(12), e2023WR034457. <https://doi.org/10.1029/2023WR034457>
- 661 Zhao, J. (2019). FluxCalR: A R package for calculating CO<sub>2</sub> and CH<sub>4</sub> fluxes from static  
662 chambers. *Journal of Open Source Software*, 4(43), 1751. <https://doi.org/10.21105/joss.01751>
- 663
- 664 Zobitz, J., Ayres, E., O'Rourke, K., Werbin, Z., Lee, L., Abdi, R., Mehmeti, D., & Xiong, L.  
665 (2024). neonSoilFlux: Compute Soil Carbon Fluxes for the National Ecological Observatory  
666 Network Sites.
- 667 Zobitz, J., & Zimmerman, N. (2025). Supporting Code and Data for neonSoilFlux: An R  
668 Package for Continuous Sensor-Based Estimation of Soil CO<sub>2</sub> Fluxes. Zenodo. <https://doi.org/10.5281/zenodo.17516320>
- 669